



PREDICTIVE MODELLING OF STRETCHABLE CONDUCTIVE INK USING FINITE ELEMENT ANALYSIS



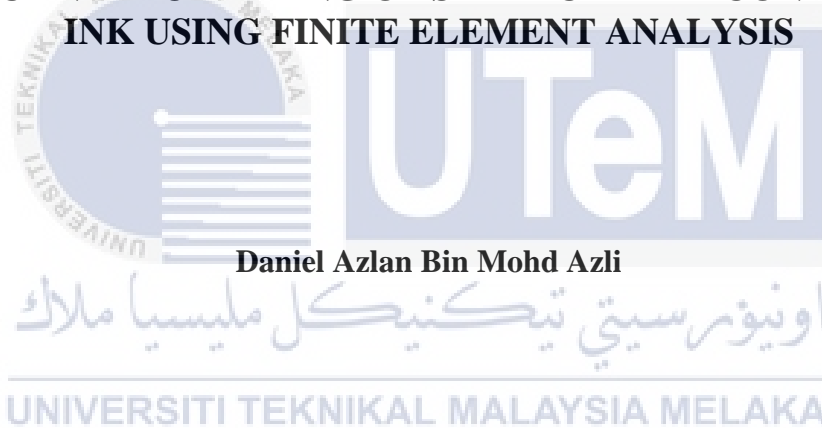
MASTER OF SCIENCE IN MECHANICAL ENGINEERING

2024



Faculty of Mechanical Technology and Engineering

**PREDICTIVE MODELLING OF STRETCHABLE CONDUCTIVE
INK USING FINITE ELEMENT ANALYSIS**



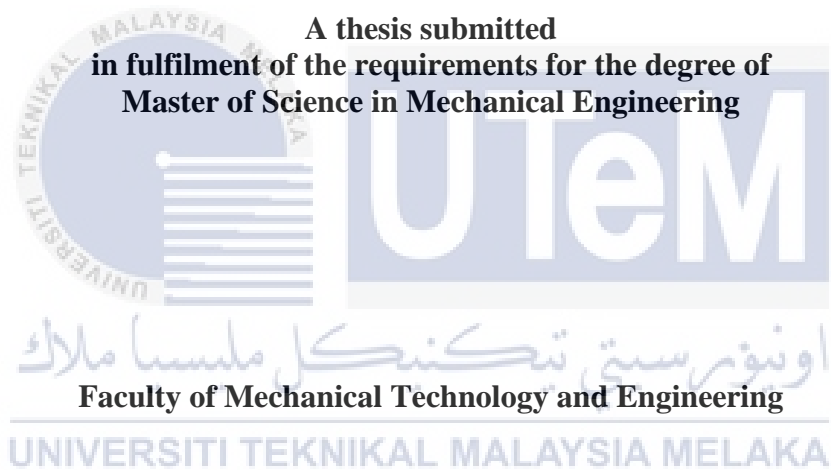
Daniel Azlan Bin Mohd Azli

Master of Science in Mechanical Engineering

2024

**PREDICTIVE MODELLING OF STRETCHABLE CONDUCTIVE INK USING
FINITE ELEMENT ANALYSIS**

DANIEL AZLAN BIN MOHD AZLI



UNIVERSITI TEKNIKAL MALAYSIA MELAKA

2024

DEDICATION

To my beloved mother and father.



ABSTRACT

Stretchable and flexible printed electronics, which utilize conductive materials made from graphene, have attracted considerable interest due to their cost-effectiveness, flexibility, and impressive ability to conform to various shapes. However, these materials often experience performance failures when subjected to strain, which poses challenges for diagnosing electrical conducting failures and predicting their behaviour. To address these issues, a numerical modelling and simulation method is needed to predict the performance of stretchable conductive ink (SCIs) based on graphene nanoplatelets (GNPs). Furthermore, when the SCI/substrate system is subjected to mechanical loadings like stretching, torsion, and bending, it can affect the functionality of the SCI, leading to electrical failures. To overcome these challenges, finite element analysis (FEA) can be employed to simulate and observe the electrical performance of the printed electronics. However, to the best of our knowledge, predictive modelling to forecast the electrical performance of the printed electronics based on the development of stress and strain energy is yet to be studied. This thesis focuses on predicting the performance of the SCI/substrate system using the FEA method. The main goal of this study was to optimize the geometrical parameters of SCI using design of experiment (DOE) software through incorporation with finite element (FE) method. In an independent study, different shapes of silver conductors (straight, zigzag, square, and sinusoidal) were compared in terms of their impact on stress, strain, and electrical performance. The straight pattern exhibited the highest average von Mises stress and maximum principal strain, while the zigzag pattern showed the lowest stress and strain. These results aligned with experimental findings, indicating that increasing stress and strain decrease the maximum strain before conductivity is lost. To validate the simulation model, input parameters were acquired by subjecting both the thermoplastic polyurethane (TPU) substrate and formulated SCI to uniaxial tensile tests. The simulated results were then compared with the experimental data, and the model exhibiting quasi-static loading with non-linear material behaviour demonstrated the closest fit with the lowest peak stress error. Lastly, the development of equivalent plastic strain was predicted using the DoE method, considering the thickness and width parameters of the conductor. Through the optimization of geometrical parameters, a printed circuit with a thickness of 0.04 mm and width of 2.66 mm was found to produce the lowest maximum equivalent plastic strain. These optimized geometrical parameters enhance the stretchability of the SCI system, allowing for greater strain tolerance and reducing the likelihood of electrical failure when subjected to mechanical deformation. In summary, this research provides insights into the performance prediction and optimization of stretchable and flexible printed electronics based on graphene conductive materials. The combination of numerical modelling, simulation, and experimental validation offers valuable tools for enhancing the reliability and functionality of these systems in various applications.

PEMODELAN RAMALAN DAKWAT KONDUKTIF BOLEH REGANG MENGUNAKAN ANALISIS UNSUR TERHINGGA

ABSTRAK

Elektronik bercetak boleh regang dan fleksibel menggunakan bahan konduktif graphene telah mendapat perhatian yang ketara kerana kosnya yang rendah, fleksibiliti dan kesesuaian yang tinggi. Walau bagaimanapun, bahan ini sering mengalami kegagalan prestasi apabila mengalami ketegangan, yang menimbulkan cabaran untuk mendiagnosis kegagalan pengalir elektrik dan meramalkan kelakuannya. Untuk menangani isu ini, kaedah pemodelan dan simulasi berangka diperlukan untuk meramalkan prestasi dakwat konduktif boleh regang (SCI) berdasarkan nanoplatelet graphene (GNP). Tambahan pula, apabila sistem SCI/substrat tertakluk kepada beban mekanikal seperti regangan, kilasan dan lenturan, ia boleh menjejaskan fungsi SCI, yang membawa kepada kegagalan elektrik. Untuk mengatasi cabaran ini, analisis unsur terhingga (FEA) boleh digunakan untuk mensimulasikan dan memerhati prestasi elektrik elektronik bercetak. Walau bagaimanapun, sepanjang pengetahuan kami, pemodelan ramalan untuk meramalkan prestasi elektrik bagi elektronik bercetak berdasarkan perkembangan tekanan dan tenaga terikan masih belum dikaji. Tesis ini memfokuskan kepada meramal prestasi sistem SCI/substrat menggunakan kaedah FEA. Matlamat utama kajian ini adalah untuk mengoptimumkan parameter geometri SCI menggunakan perisian reka bentuk eksperimen (DOE) melalui penggabungan dengan kaedah unsur terhingga (FE). Dalam kajian bebas, bentuk konduktor perak yang berbeza (lurus, zigzag, segi empat sama dan sinusoidal) telah dibandingkan dari segi kesannya terhadap tekanan, terikan dan prestasi elektrik. Corak lurus menunjukkan tekanan von Mises purata tertinggi dan regangan prinsipal maksimum, manakala corak zigzag menunjukkan tegasan dan regangan yang paling rendah. Keputusan ini sejajar dengan penemuan eksperimen, menunjukkan bahawa peningkatan tegasan dan terikan mengurangkan terikan maksimum sebelum kekonduksian hilang. Untuk mengesahkan model simulasi, parameter input diperolehi dengan menundukkan kedua-dua substrat poliuretana termoplastik (TPU) dan merumuskan SCI kepada ujian tegangan uniaxial. Hasil simulasi kemudiannya dibandingkan dengan data eksperimen, dan model yang mempamerkan pemuatan kuasi statik dengan gelagat bahan bukan linear menunjukkan kesesuaian paling hampir dengan ralat tegasan puncak terendah. Akhir sekali, perkembangan terikan plastik yang setara telah diramalkan menggunakan kaedah DoE, dengan mengambil kira ketebalan dan parameter lebar konduktor. Melalui pengoptimuman parameter geometri, litar bercetak dengan ketebalan 0.04 mm dan lebar 2.66 mm didapati menghasilkan regangan plastik setara maksimum yang paling rendah. Parameter geometri yang dioptimumkan ini meningkatkan keanjalan sistem SCI, membolehkan toleransi terikan yang lebih besar dan mengurangkan kemungkinan kegagalan elektrik apabila mengalami ubah bentuk mekanikal. Ringkasnya, penyelidikan ini memberikan pandangan tentang ramalan prestasi dan pengoptimuman elektronik bercetak boleh regang dan fleksibel berdasarkan bahan konduktif graphene. Gabungan pemodelan berangka, simulasi dan pengesahan eksperimen menawarkan alat berharga untuk meningkatkan kebolehpercayaan dan kefungsi sistem ini dalam pelbagai aplikasi.

ACKNOWLEDGEMENTS

In the name of Allah, The Lord, The Most Beneficial and The Merciful

All thanks belong to Allah, the Most Gracious, the Most Merciful and the source of this success to complete this thesis.

I am immensely grateful to my supervisor, Dr. Mizah Binti Ramli, for her unwavering support, valuable guidance, and expert advice. Her encouragement and insightful feedback have been invaluable in shaping the direction of my research. I would also like to express my heartfelt appreciation to my co-supervisor, Dr. Mohamad Shukri Bin Zakaria, for his assistance during the simulation procedure employing the finite element analysis method. His expertise and dedication have greatly contributed to the success of this project.

I would like to acknowledge the pivotal role of Prof. Ir. Ts. Dr. Ghazali bin Omar, the project leader, and the entire team of lecturers associated with Collaborative Research in Engineering, Science, and Technology (CREST). Their collective knowledge, guidance, and encouragement have been instrumental in the realization of this research endeavor. I extend my gratitude to CREST, under project code I00053, for providing the necessary funding and support for this project. Additionally, I would like to acknowledge the financial assistance received through the ZAMALAH scholarship scheme from Universiti Teknikal Malaysia Melaka (UTeM).

I am deeply grateful to my colleagues, Zuraimi Bin Ramle and Andee Faeldza Bin Dziaudin, who have been with me throughout this research project. Their collaboration, valuable discussions, and assistance have been pivotal in overcoming challenges and achieving meaningful results. My sincere appreciation goes to everyone from the Advanced Materials and Characterization Laboratory (AMCHAL). Their technical support, resources, and collaborative spirit have been vital in the experimental aspects of this research. I would like to express my gratitude to the Faculty of Mechanical Engineering for providing access to the necessary laboratory equipment, which has greatly facilitated the experimental work carried out for this thesis.

I would like to extend my special thanks to my family, especially my beloved mother, father, and siblings, for their unwavering support, encouragement, and understanding throughout this academic pursuit. Additionally, I am grateful to my partner for their continuous support, love, and understanding during this demanding period. Lastly, I would like to express my gratitude to everyone associated within the crucial parts of the realization of this project. Your contributions, whether big or small, have played a significant role in the successful completion of this master thesis.

Thank you all for your unwavering support and guidance throughout this journey.

TABLE OF CONTENTS

	PAGE
DECLARATION	
APPROVAL	
DEDICATION	
ABSTRACT	i
ABSTRAK	ii
ACKNOWLEDGEMENTS	iii
TABLE OF CONTENTS	iv
LIST OF TABLES	vii
LIST OF FIGURES	ix
LIST OF ABBREVIATIONS	xiv
LIST OF SYMBOLS	xviii
LIST OF PUBLICATIONS	xxi
CHAPTER	
1. INTRODUCTION	1
1.1 Background	1
1.2 Problem statement	7
1.3 Objective	9
1.4 Research scopes	9
2. LITERATURE REVIEW	10
2.1 Introduction to stretchable electronics	10
2.2 Type of conductive ink fillers	14
2.2.1 Metal-based fillers	14
2.2.2 Conducting polymers	16
2.2.3 Carbon-based/ nanocarbon-based fillers	18
2.2.4 Hybrid conductive fillers	26
2.3 Polymer binder	28
2.3.1 Epoxy	30
2.3.2 Poly(3,4-ethylenedioxythiophene): polystyrene sulfonate	31
2.4 Solvent	33
2.4.1 Dimethyl sulfoxide	34
2.5 Surfactant	35
2.5.1 Polyoxyethylene octyl phenyl ether	36
2.5.2 Ethylene glycol	37
2.6 Stretchable and flexible substrates	38
2.6.1 Stretchable thermoplastic urethane substrate	39
2.6.2 Flexible polyethylene terephthalate substrate	40
2.7 Mixing process	42
2.8 Printing process	43
2.9 Curing process	46

2.10	Nanoindentation testing	47
2.11	Experimental study of stretchability for SCI	48
2.12	Electromechanical effect towards stretchability limit	49
2.13	Stretchability performance through finite element analysis	52
2.14	Performance prediction through finite element analysis	57
2.15	Finite element analysis for stretchable conductive ink performance	61
2.16	Validation and optimization of simulation model	62
3.	METHODOLOGY	64
3.1	Introduction	64
3.2	Raw materials	65
3.2.1	Conductive filler	66
3.2.2	Conductive polymer binder	67
3.2.3	Solvents	68
3.2.4	Substrate materials	70
3.3	Formulation of stretchable conductive ink	71
3.4	Sample preparation	74
3.4.1	GNP/PEDOT: PSS stretchable conductive ink	74
3.4.2	Sample preparation for mechanical testing	76
3.5	Printing process	79
3.5.1	Fabrication of stencil	83
3.5.2	Deposition of conductive ink through stencil printing	84
3.6	Curing process	84
3.7	Mechanical testing through dynamic mechanical analysis	86
3.7.1	Viscosity test	87
3.7.2	Nanoindentation test	88
3.7.3	Quasi-static uniaxial tensile test	91
3.8	Electrical characterization	92
3.9	FE Modelling of SEC	93
3.9.1	FE model	94
3.9.2	Mesh convergence study	94
3.9.3	Boundary conditions	95
3.9.4	Contact properties between ink and substrate	98
3.9.5	Material properties under validation method	99
3.9.6	Validation of finite element model	99
3.10	Validation and optimization of simulation model	102
4.	RESULTS AND DISCUSSION	105
4.1	Introduction	105
4.2	Effect of filler and substrate on electrical resistivity	106
4.3	Effect of filler sizes on electrical performance	109
4.4	Viscosity of SCI	111
4.5	Results of mechanical testing via UTM	113
4.5.1	Uniaxial tensile test of TPU substrates	113

4.5.2	Uniaxial tensile test of bulk GNP/PEDOT: PSS SCI specimen	115
4.5.3	Nanoindentation of GNP/PEDOT: PSS SCI	118
4.6	Comparison between simulation and experimental study	122
4.6.1	Results of mesh convergence study in simulation	123
4.6.2	Maximum VMS distribution on patterns for uniaxial loading	125
4.6.3	Maximum VMS distribution on patterns for biaxial loading	130
4.6.4	Maximum principal strain of each pattern for uniaxial loading	134
4.7	Validation of FE model	143
4.7.1	Validation of TPU model through comparison with experiment	144
4.8	Predictive modelling of maximum equivalent plastic strain	146
4.9	Optimization of the geometrical parameters	150
5.	CONCLUSION AND RECOMMENDATIONS	154
5.1	Conclusion of the study	154
5.2	Recommendation for future study	155
	REFERENCES	157



LIST OF TABLES

TABLE	TITLE	PAGE
Table 1.1	Advantages and disadvantages of metals as filler for SCI	3
Table 2.1	Intrinsic electrical resistivity and conductivity of common metal-based fillers	16
Table 2.2	Structure of conducting polymers in undoped form	17
Table 2.3	Differences between graphite and graphene	24
Table 2.3	Maximum elongation rate before each pattern starts losing its conductivity (Yunos et al., 2020b).	50
Table 2.4	The geometrical parameters, thickness, and width, used by past researchers for the design of electronic circuits, with reference to the related literature	60
Table 3.1	Specifications of the commercially available GNP fillers	67
Table 3.2	Specification of commercially available PEDOT: PSS with 1.3 wt.% dispersion in H ₂ O.	68
Table 3.3	Properties of DMSO and Triton x-100	69
Table 3.4	Properties of EG	70
Table 3.5	Specification of commercially available TPU and PET substrate	70
Table 3.6	Formulation of GNP/PEDOT: PSS SCI subjected to three different fillers and matrix loading	73
Table 3.7	Synthesis of PEDOT: PSS solution	73
Table 3.8	Different phases of GNP fillers varied at different ratios and weight percentages used in formulation of SCI	76
Table 3.9	Test conditions during the nanoindentation procedure of the printed GNP/PEDOT: PSS SCI on top of glass substrate	89

Table 3.10	Properties of ink and substrate used in the simulation (Mohammed, 2017)	94
Table 3.11	Sets of combinations for geometrical parameters designed through DoE software.	104
Table 4.1	Modulus of elasticity obtained at each point of nanoindentation	121
Table 4.2	Number of nodes and elements generated from the meshing results of each pattern	124
Table 4.3	Tabulation of VMS for uniaxial longitudinal tensile loading of all the patterns	126
Table 4.4	Tabulation of VMS for uniaxial lateral loading of all the patterns	128
Table 4.5	Tabulation of VMS for biaxial loading of all the patterns	131
Table 4.6	Tabulation of new VMS for biaxial loading of all the patterns	132
Table 4.7	Tabulation MPS and percentage of strain reduction for uniaxial longitudinal and lateral tensile loading of all the patterns	136
Table 4.8	Tabulation of new MPS and percentage strain reduction for biaxial tensile loading of all patterns	141
Table 4.9	Maximum equivalent plastic strain obtained for each set of numerical factors	147
Table 4.10	ANOVA for maximum equivalent plastic strain model	150
Table 4.11	Criterion for the optimization process of the geometrical parameters	151
Table 4.12	Optimization criteria for geometrical parameters using DoE software	152

LIST OF FIGURES

FIGURE	TITLE	PAGE
Figure 1.1	Simple printed circuit board (PCB)	2
Figure 1.2	Carbon allotropes for graphite and diamond	4
Figure 2.1	Diversity of applications for stretchable electronics	13
Figure 2.2	Raw materials of (a) silver, (b) copper and (c) gold	15
Figure 2.3	Carbon allotrope of CNT	19
Figure 2.4	Percolated network of CNT fibres within a composite system (Taya et al., 1998)	19
Figure 2.5	Atomic structure of graphene	23
Figure 2.6	Atomic structure of graphite and graphene	23
Figure 2.7	Electron band structure of (a) graphite materials (semiconductor) and (b) insulators	25
Figure 2.8	Chemical bonding of PEDOT: PSS conducting polymer	31
Figure 2.9	Schematic core-shell structure of PEDOT: PSS	32
Figure 2.10	Chemical composition of DMSO	35
Figure 2.11	Chemical composition of Triton X-100 (Geng et al., 2008)	36
Figure 2.12	Behaviour of TPU substrate after being applied with different types of mechanical forces (Wagner and Bauer, 2012)	40
Figure 2.13	Molecular composition of PET	41
Figure 2.14	Some of the applications made through printing process of conductive nanomaterials (Li et al., 2019)	43
Figure 2.15	Accumulation of plastic strain of wavy patterns (horseshoe) (a) at edge of single line-track and (b) at edge of multi-line track	54

Figure 2.16	All the designs employed for the edge of zigzag by Kim et al. (2021)	56
Figure 2.17	Maximum equivalent stress at cross-section A-A for biaxial tensile loading	57
Figure 3.1	Flow chart of the methodologies used during the research work	65
Figure 3.2	Commercially available PEDOT: PSS obtained from Sigma Aldrich	67
Figure 3.3	Flowchart for the sample preparation procedure of SCI	75
Figure 3.4	Schematic diagram of the geometries for dog-bone base plate viewed at (a) top view, (b) side view, (c) isometric view, and (d) bottom view	78
Figure 3.5	Schematic diagram of the geometries for rectangular base plate viewed at (a) top view, (b) side view, (c) isometric view, and (d) bottom view	78
Figure 3.6	Top and side view of the TPU	79
Figure 3.7	Complete diagram for the methods used for the whole printing process of a complete printed circuit of SCI	81
Figure 3.8	PET/ substrate stacking using PET as stencil for stencil printing of SCI circuit	82
Figure 3.9	Dimensions of the aperture designed through SolidWorks for (a) straight pattern, (b) sinusoidal pattern, (c) square pattern, (d) zigzag pattern, and (e) simple circuit design	83
Figure 3.10	Procedure for doctor-blading method in printing SCI	84
Figure 3.11	Sheet resistivity of the printed SCI on top of two different substrates cured at various temperatures	86
Figure 3.12	52DV Digital Viscometer	87
Figure 3.13	Sea-level placement of the GNP/PEDOT: PSS SCI	88
Figure 3.14	Printed GNP/PEDOT: PSS SCI on top of glass substrate used during nanoindentation procedure.	90
Figure 3.15	Dimension for one sample of printed SCI utilized for the nanoindentation procedure viewed from top.	90
Figure 3.16	Depiction of the probe head is situated atop the SCI surface	93
Figure 3.17	Schematic diagram of the model at the application of BC1, BC2, and BC3 for (a) longitudinal and (b) lateral loading. The	96

fixed end and loading point location are denoted by the dotted line and arrow, respectively. All the patterns employed the same boundary conditions

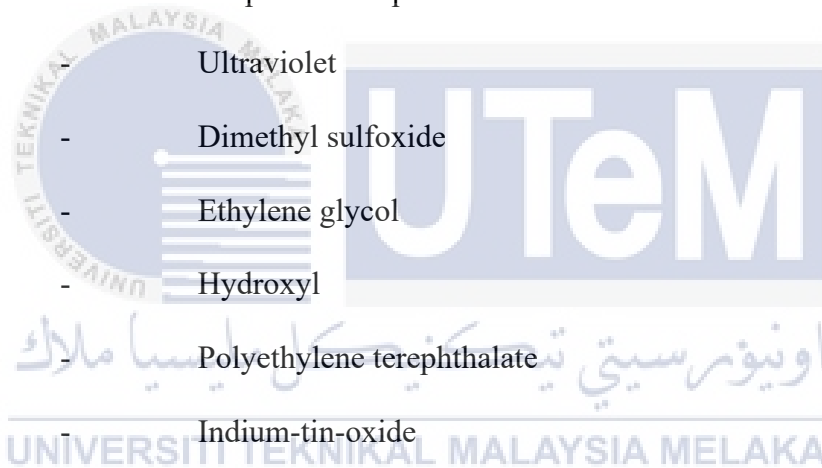
Figure 3.18	Applied boundary conditions for the model implementing the biaxial tensile loading	97
Figure 3.19	(a) Schematic diagram of the quasi-static tensile test using universal tensile testing machine and (b) Regions of applied boundary conditions for TPU modelling	100
Figure 3.20	Circuit geometry with 0.5 mm width designed using SolidWorks	103
Figure 4.1	Average sheet resistivity obtained by printing the SCI at three different filler loadings on top of two different plastic substrates	107
Figure 4.2	Sheet resistivity of the distinct size of GNPs filler at varied weight percentages of SCI ink	110
Figure 4.3	Sheet resistivity of the distinct size of GNPs filler at varied ratios	111
Figure 4.4	Effect of increasing GNPs filler loading towards the viscosity of the GNP/PEDOT: PSS SCI	112
Figure 4.5	Comparison of the experimentally stretched S-S curve for all the TPU substrates	114
Figure 4.6	S-S curve for the bulk of GNP/PEDOT: PSS SCI – Specimen 1	116
Figure 4.7	S-S curves for the second bulk specimen of GNP/PEDOT: PSS SCI	117
Figure 4.8	Minimum-maximum normalization plot for two specimens of bulk GNP/PEDOT: PSS SCI	118
Figure 4.9	Load-displacement curves of the printed GNP/PEDOT: PSS SCI at two holding time	119
Figure 4.10	Load-displacement curves tested at 10 points	121
Figure 4.11	Graph of mesh convergence study for two patterns chosen; straight and zigzag	125
Figure 4.12	The stress distributions when subjected to uniaxial longitudinal tensile loading for (a) straight, (b) sinusoidal, (c) zigzag, and (4) square pattern, respectively	127

Figure 4.13	The stress distributions when subjected to uniaxial lateral tensile loading for (a) straight, (b) sinusoidal, (c) zigzag, and (4) square pattern, respectively	129
Figure 4.14	(a) Localisation of high-stress value on zigzag ink pattern occurring at the tip of the outer edge of the zigzag pattern and (b) Localisation of high-stress value on sinusoidal ink pattern occurring at the tip of the outer crest and trough of the sinusoidal pattern	130
Figure 4.15	The stress distributions when subjected to biaxial tensile loading for (a) straight, (b) sinusoidal, (c) zigzag, and (4) square pattern, respectively	133
Figure 4.16	The location of the occurrence of the maximum VMS for (a) straight, (b) square, (c) sinusoidal, and (d) zigzag pattern. The black dashed lines represent the cutting line for each pattern to simplify the model of the ink	133
Figure 4.17	The contour plot depicts the maximum principal strain distribution under uniaxial longitudinal tensile loading for various patterns: (a) straight, (b) sinusoidal, (c) zigzag, and (d) square. Figures on the left ((a) – (d)) display the maximum principal strain across the entire model for each pattern, while those on the right reveal the maximum principal strain specific to the stand-alone patterns	137
Figure 4.18	Contour plot of the maximum principal strain distribution (left) under uniaxial lateral tensile loading for a pattern of (a) straight, (b) sinusoidal, (c) zigzag, and (d) square and their location of high principal strain (right).	139
Figure 4.19	Contour plot of the maximum principal strain distribution (left) under biaxial tensile loading for a pattern of (a) straight, (b) sinusoidal, (c) zigzag, and (d) square and their locations of high principal strain magnitude.	143
Figure 4.20	Comparison of the S-S curve of different simulation models with experimental results	144
Figure 4.21	Region of high concentration of maximum equivalent plastic strain for 1.75 mm wide and 0.01 mm thick SCI model viewed at (a) SCI/ substrate system and (b) independent SCI model	148
Figure 4.22	Interaction and pattern of slope between (a) maximum equivalent plastic strain against thickness and (b) maximum equivalent plastic strain against width	149

LIST OF ABBREVIATIONS

PCB	-	Printed circuit board
SMB	-	Small medium business
SCI	-	Stretchable conductive ink
CNT	-	Carbon nanotube
0-D	-	0-dimension
1-D	-	1-dimension
2-D	-	2-dimension
CP	-	Conducting polymers
AMOLED	-	Active-matrix organic light-emitting diode
OLED	-	Organic light-emitting diode
SEC	-	Stretchable electronic circuit
RFID	-	Radio-frequency identification device
EEG	-	Electroencephalogram
ECG	-	Electrocardiogram
PPy	-	Polypyrrole
PANI	-	Polyaniline
PT	-	Polythiophene
PPV	-	Poly(p-phenylenevinylene)
PEDOT	-	Poly(3,4-ethylenedioxythiophene)
PSS	-	Poly(styrene sulfonic acid)

LED	-	Light-emitting diode
COOH	-	Carboxylic acid
SWCNT	-	Single-walled carbon nanotube
MWCNT	-	Multi-walled carbon nanotube
PEG	-	Polyethylene glycol
LPE	-	Liquid-phase exfoliation
CVD	-	Chemical vapor deposition
GO	-	Graphene oxide
RGO	-	Reduced graphene oxide
GNP	-	Graphene nanoplatelet
UV	-	Ultraviolet
DMSO	-	Dimethyl sulfoxide
EG	-	Ethylene glycol
OH	-	Hydroxyl
PET	-	Polyethylene terephthalate
ITO	-	Indium-tin-oxide
RHCP	-	Right-hand circularly polarized
PDMS	-	Polydimethylsiloxane
FTCF	-	Flexible transparent conductive films
TPU	-	Thermoplastic polyurethane
TPE	-	Thermoplastic elastomers
FEA	-	Finite element analysis
NW	-	Nanowire
DOE	-	Design of experiment
DMA	-	Dynamic mechanical analysis



S-S	-	Stress-strain
ASTM	-	American society for testing and materials
FE	-	Finite element
UTM	-	Universal tensile machine
FTIR	-	Fourier-transform infra-red
VMS	-	Von mises stress
BC	-	Boundary condition
BC1	-	Boundary condition at fixed end $x = 0$ mm for longitudinal loading and $y = 0$ mm at lateral loading
BC2	-	Constraint from rotational displacement in all directions and translational displacement normal to the model
BC3	-	Reference point at the center of the cross-sectional area opposite to BC1
CAE	-	Complete Abaqus environment
DMA	-	Dynamic mechanical analysis
RF	-	Reference point
C3D8R	-	8-node linear brick element featuring reduced integration and hourglass system
IGES	-	Initial graphics exchange specifications
STEP	-	Standard for the exchange of product data
SCP	-	Suspended colloidal particles
PUF	-	Phenol-urea-formaldehyde
TPU_1	-	First sample of bulk TPU
TPU_2	-	Second sample of bulk TPU
TPU_3	-	Third sample of bulk TPU

MPS	-	Maximum principal strain
ANOVA	-	Analysis of variance



LIST OF SYMBOLS

Cu	-	Copper
Ag	-	Silver
Au	-	Gold
F	-	Volume of conductive fillers
f^*	-	Threshold volume fraction of fillers
σ_f	-	Conductivity of fiber
σ_c	-	Conductivity of composite
T	-	Conductivity exponent
R	-	Resistance
Tn	-	Tin
Zn	-	Zinc
R_s	-	Sheet resistance
R_0	-	Initial resistance
V	-	Volume fraction or weight percentage of filler
C	-	Composite
P	-	Particulate phase
M	-	Matrix
V_m	-	Volume fraction of PEDOT: PSS solution
E	-	Elastic modulus or Young's modulus
F	-	Minimum force

V_L	-	Loading speed
T	-	Holding time
D	-	Indentation depth
G	-	Correction factor
V	-	Voltage
I	-	Current
σ_1	-	Principal stress in x-axis
σ_2	-	Principal stress in y-axis
σ_3	-	Principal stress in z-axis
Σe	-	Equilibrium stress
μ	-	Poisson's ratio
ϵ_1	-	Principal strain in x-axis
ϵ_2	-	Principal strain in y-axis
ϵ_3	-	Principal strain in z-axis
ϵ_{yt}	-	Yield point strain
σ_{yt}	-	Yield point stress
∂_z	-	Expansion of the simulation model
θ_z	-	Contraction of the simulation model
ΔL_x	-	Total displacement for longitudinal stretch of biaxial load (3.0 mm)
ΔL_y	-	Total displacement for lateral stretch of biaxial load (9.5 mm)
ΔL_{x1}	-	Positive longitudinal stretch = 9.5 mm (uniaxial loading) and 1.5 mm (biaxial loading)
ΔL_{y1}	-	Positive lateral stretch = 3.0 mm (uniaxial loading) and 4.75 mm (biaxial loading)

ΔL_{x2}	-	Negative longitudinal stretch = 1.5 mm (biaxial loading)
ΔL_{y2}	-	Negative lateral loading = 4.75 mm (biaxial loading)
ΔL_{total}	-	Total displacement of biaxial tensile loading
$\sigma_{TPU,max}$	-	Highest peak stress among three TPUs
$\bar{\sigma}_{TPU}$	-	Average peak stress of three TPUs
$\sigma_{TPU,min}$	-	Lowest peak stress among three TPUs
Ω/sq	-	Ohm/square
$\Omega.m$	-	Ohm meter
Σ	-	Population standard deviation
x_i	-	Individual value from population
M	-	Mean of the population
N	-	Sample size of the population
$\sigma_{max,1}$	-	Peak normalized stress for the first specimen of bulk GNP/PEDOT: PSS ink
$\sigma_{max,2}$	-	Peak normalized stress for the second specimen of bulk GNP/PEDOT: PSS ink
σ_{avg}	-	Average Von Mises stress for elastic model
σ_{max}	-	Maximum Von Mises stress for elastic model
σ_{min}	-	Minimum Von Mises stress for elastic model
E_i	-	Input strain

LIST OF PUBLICATIONS

Azli, D.A.M., Zakaria, M.S., Ramli, M., Omar, G., Nordin, M.N.A., Syaifuddin, S., Ramle, Z., Dziaudin, A.F. and Abdullah, A.H.L., 2023. Equivalent Plastic-Strain Analysis of Copper Stretchable Electronic Circuit Using Finite Element Analysis. *Journal of Advanced Research in Applied Sciences and Engineering Technology*, 30, 31-43.

Azli, D.A.M., Ramli, M., Zakaria, M.S., Nordin, M.N.A., Omar, G., Ghazaly, M.M. and Abdullah, A.H.L., 2021. The Impact of Stress Distribution on The Electrical Performance of Different Silver Stretchable Conductive Ink Pattern Using FEA Simulation. *International Journal of Nanoelectronics and Materials*, 14, 209-218.

UNIVERSITI TEKNIKAL MALAYSIA MELAKA